











Expanding RNAi therapeutics to extrahepatic tissues with lipophilic conjugates

Kirk M. Brown^{1,2}, Jayaprakash K. Nair^{1,2}, Maja M. Janas^{1,2}, Yessenia I. Anglero-Rodriguez¹, Lan T. H. Dang¹, Haiyan Peng¹, Christopher S. Theile¹, Elena Castellanos-Rizaldos¹, Christopher Brown¹, Donald Foster¹, Jeffrey Kurz¹, Jeffrey Allen¹, Rajanikanth Maganti¹, Jing Li¹, Shigeo Matsuda¹, Matthew Stricos¹, Tyler Chickering¹, Michelle Jung¹, Kelly Wassarman¹, Jeff Rollins¹, Lauren Woods¹, Alex Kelin¹, Dale C. Guenther¹, Melissa W. Mobley¹, John Petrulis¹, Robin McDougall¹, Timothy Racie¹, Jessica Bombardier¹, Diana Cha¹, Saket Agarwal¹, Lei Johnson¹, Yongfeng Jiang¹, Scott Lentini¹, Jason Gilbert¹, Tuyen Nguyen¹, Samantha Chigas¹, Sarah LeBlanc¹, Urjana Poreci¹, Anne Kasper¹, Arlin B. Rogers¹, Saeho Chong¹, Wendell Davis¹, Jessica E. Sutherland¹, Adam Castoreno¹, Stuart Milstein¹, Mark K. Schlegel¹, Ivan Zlatev¹, Klaus Charisse¹, Mark Keating¹, Muthiah Manoharan¹, Kevin Fitzgerald¹, Jing-Tao Wu¹, Martin A. Maier¹[✉] and Vasant Jadhav¹[✉]

Therapeutics based on short interfering RNAs (siRNAs) delivered to hepatocytes have been approved, but new delivery solutions are needed to target additional organs. Here we show that conjugation of 2'-O-hexadecyl (C16) to siRNAs enables safe, potent and durable silencing in the central nervous system (CNS), eye and lung in rodents and non-human primates with broad cell type specificity. We show that intrathecally or intracerebroventricularly delivered C16-siRNAs were active across CNS regions and cell types, with sustained RNA interference (RNAi) activity for at least 3 months. Similarly, intravitreal administration to the eye or intranasal administration to the lung resulted in a potent and durable knockdown. The preclinical efficacy of an siRNA targeting the amyloid precursor protein was evaluated through intracerebroventricular dosing in a mouse model of Alzheimer's disease, resulting in amelioration of physiological and behavioral deficits. Altogether, C16 conjugation of siRNAs has the potential for safe therapeutic silencing of target genes outside the liver with infrequent dosing.

RNA interference (RNAi) therapeutics use an endogenous mechanism whereby short interfering RNAs (siRNAs) direct the RNA-induced silencing complex (RISC) to sequence matched target transcripts for knockdown¹. Both lipid nanoparticles and *N*-acetylgalactosamine (GalNAc) conjugates are clinically validated and approved delivery strategies for liver targets^{2–8}. Building on nearly 2 decades of siRNA design and chemistry optimization^{9–12}, we demonstrate here that, with suitable delivery solutions, the RNAi pathway can be harnessed in extrahepatic tissues, such as the central nervous system (CNS), eye and lung. Multiple CNS diseases, representing some of the highest unmet medical needs and greatest therapeutic challenges, have been associated with dominant gain-of-function mutations, making them suitable candidates for an RNAi-based silencing approach. As such, chemically modified siRNAs have demonstrated potent and sustained silencing in rodents and non-human primates (NHPs); however, using an invasive intracerebroventricular (ICV) administration approach¹³ that is not suitable for repeated dosing in humans. Furthermore, technologies enabling siRNA delivery across the blood–brain barrier following a less challenging systemic administration are similarly being explored^{14–17}, which are, however, still in early stages of discovery. In the eye, intravitreal (IVT) dosing of siRNAs has been evaluated in late-stage clinical studies, with few safety concerns, but did not advance further due to lack of efficacy¹⁸. Recently, the

Coronavirus Disease 2019 (COVID-19) pandemic has highlighted the importance of optimizing siRNA delivery to the lung for the treatment of emergent viral respiratory diseases. Although earlier programs have already shown potential clinical benefits of siRNA-based therapeutics in the lung¹⁹, 2'-O-hexadecyl (C16) conjugates demonstrate enhanced delivery and siRNA uptake into the alveolar and bronchiolar epithelium. Taken together, this work highlights that the combination of a C16 lipophilic modification with our fully chemically modified, metabolically stable siRNAs achieves efficient delivery to the CNS, eye and lung, resulting in a robust and durable gene silencing in rodents and NHPs, with a favorable safety profile. We think that these advances have the potential to generate multiple candidates for investigating clinical safety and efficacy in humans.

Results

Optimization of the siRNA conjugate design. Lipophilic moieties represent one of the earliest approaches to improve cellular uptake and delivery of antisense oligonucleotides (ASOs) and siRNAs to the liver and various other organ systems²⁰, including the CNS^{21–23}. We reasoned that, by carefully optimizing the lipophilicity of chemically modified siRNAs, we could enhance intracellular delivery without compromising broad biodistribution, potency and safety. We used the 2' position of the ribose sugar backbone to introduce

¹Alnylam Pharmaceuticals, Cambridge, MA, USA. ²These authors contributed equally: Kirk M. Brown, Jayaprakash K. Nair, Maja M. Janas.

✉e-mail: mmaier@alnylam.com; vjadhav@alnylam.com

the lipophilic moiety, as it provides many options for the positioning of the lipophile within the siRNA duplex.

The lipophile was introduced at the N6 (position 6 from the 5' end) of the sense strand, and the effect of its chain length was evaluated in the rat CNS using a superoxide dismutase 1 (*Sod1*)-targeting siRNA (Supplementary Table 1). The RNAi activity of siRNA conjugates in the CNS generally increased with lipid chain length, with C16 providing optimal activity in the rat spinal cord and brain at 2 weeks after an intrathecal (IT) dose (Fig. 1a). To determine the positional effect, C16 was walked across both strands of the siRNA and screened via transfection in RPE-J cells (Fig. 1b). The C16 conjugation was well-tolerated across both strands, with potency similar to the unconjugated siRNA, except for a few positions known to be sensitive to sterically demanding 2' modifications⁹. A subset of the C16-siRNAs was selected for in vivo evaluation in rats via a single 0.9-mg IT dose. Most tested positions provided activity equivalent to the sense strand N6 after 1 month (Fig. 1c), confirming positional tolerance of C16 modification. In vitro-in vivo discrepancy was observed with the antisense strand N16 conjugate, potentially due to a metabolic liability in vivo that affected the duration. The sense strand N6 was chosen to maintain functional RISC activity and to reduce the risk of exonuclease-mediated cleavage of the conjugate from termini.

Next, we confirmed that known siRNA design elements, such as the strategic placement of 2'-fluoro and 2'-O-methyl chemical modifications to increase potency⁹, or glycol nucleic acid (GNA) in the antisense seed region to increase specificity^{10,24}, retained similar benefits in the CNS (Fig. 1d). Furthermore, we assessed the relative importance of C16 and/or 5'-(E)-vinylphosphonate (VP), a 5' phosphate mimic placed at the 5' end of the antisense strand to promote RISC loading²⁵, on potency (Fig. 1e). Although the addition of either C16 or VP produced a robust mRNA knockdown in the spinal cord (up to 80%), only a modest knockdown in the brain (up to 50%) was observed. The siRNA combining both VP and C16 had the best activity across CNS regions, with up to 90% and 75% mRNA knockdown in the spinal cord and brain, respectively. There was no activity in the rat striatum, liver and kidney at the tested dose level and time point. Consistent with the functional knockdown data across CNS regions, the C16-siRNA demonstrated superior brain biodistribution compared to its unconjugated version after a single IT injection in rats (Fig. 1f).

C16 conjugation enables broad and efficient siRNA delivery to the rodent CNS. To understand C16-siRNA uptake and RNAi activity across the major CNS cell types, we designed siRNAs against cell-type-specific targets uniquely expressed in neurons (*Map2*), astrocytes (*Gfap*), microglia (*Iba1*) or oligodendrocytes (*Mbp*) and the endothelium/perivascular macrophages (*Pecam1*) (Supplementary Table 1). After an IT dose in rats, immunohistochemistry (IHC) to detect siRNAs revealed widespread drug

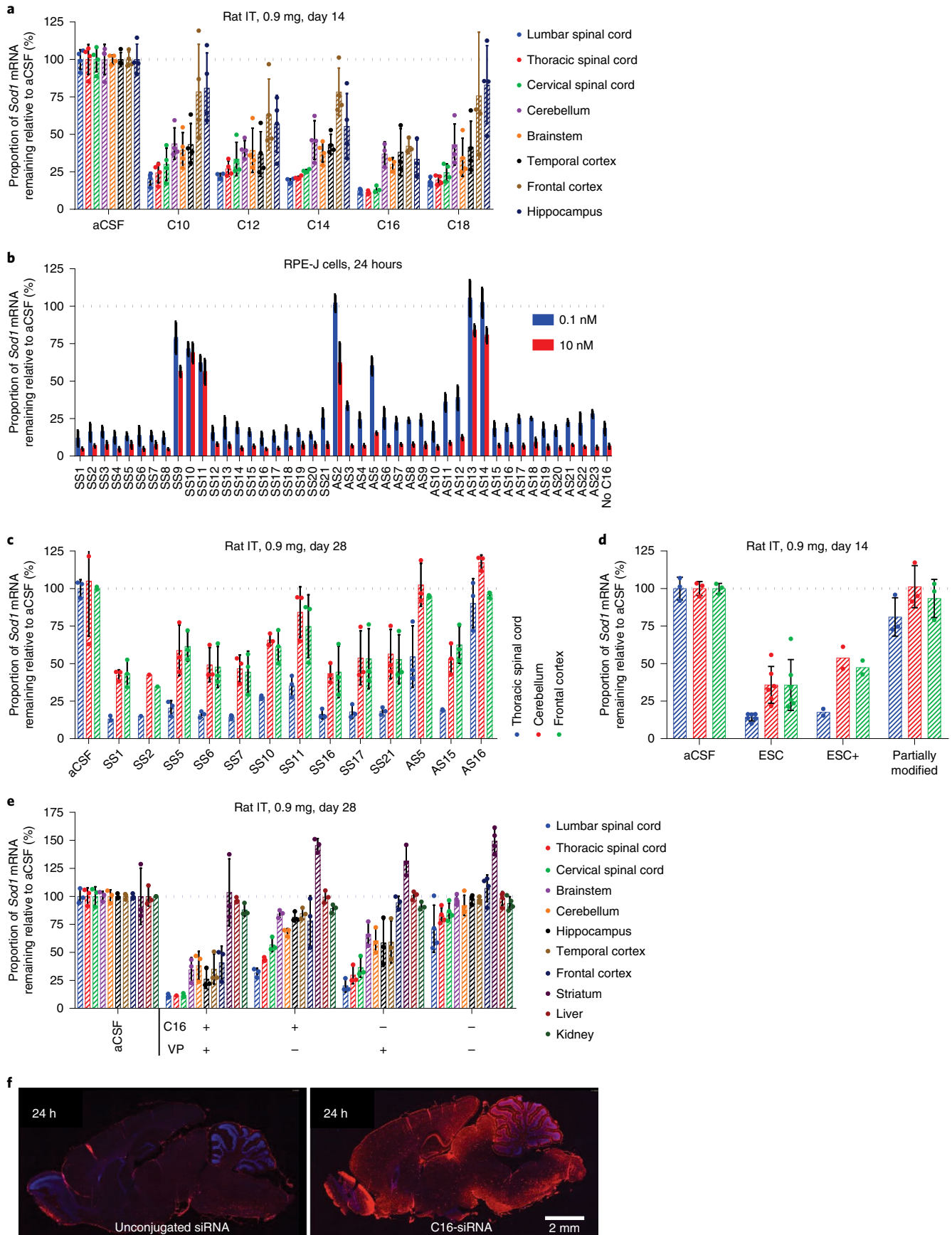
distribution in neurons and glial cells (Fig. 2a). Dual IHC confirmed cell-specific uptake in neurons, astrocytes and microglial cells (Fig. 2a), whereas siRNA accumulation in oligodendrocytes was below the IHC limit of detection (Fig. 2a). Robust knockdown was observed in neurons, astrocytes and microglia (Fig. 2b), whereas it was less effective in oligodendrocytes, consistent with lower siRNA exposure. Vascular endothelium and perivascular macrophages did not show functional RNAi activity (Fig. 2b). Overall, these data indicate that C16-siRNAs are productively taken up by most CNS cell types of therapeutic relevance.

Knockdown of *Sod1* mRNA was dose dependent in the spinal cord and the brain (Fig. 2c). The duration of knockdown was assessed in a 6-month study in rats after a single 0.9-mg IT dose (Fig. 2d). In the lower spinal cord, the maximal level of target knockdown was observed as early as 1 week post-dose (earliest time point tested), with sustained silencing out to 6 months. Brain regions analyzed showed >75% silencing for at least 3 months with partial recovery out to 6 months, except for the temporal cortex where *Sod1* expression started to recover at 2 months post-dose. One additional cohort of rats received multiple doses of 0.3 mg at approximately monthly intervals for up to five doses, with the last group killed at 2 weeks post-final-dose (4.5 months after the first dose) (Fig. 2e). Silencing appeared to be additive, with similar *Sod1* knockdown in the frontal cortex, cerebellum and cervical spinal cord at 1 month after three 0.3 mg doses versus a single 0.9 mg dose at the same time point (Fig. 2d). Knockdown appeared to recover in the thoracic spinal cord after 3 months in the multi-dose rat IT study (Fig. 2e), which is inconsistent with the 6-month single-dose rat IT data with the same C16-siRNA (Fig. 2d), and the other CNS regions of the same experiment, and may be due to assay or technical variability.

Dose-dependent silencing in the frontal cortex correlated with drug exposure (Fig. 2f), with the siRNA half-life for the 0.9 mg group calculated to be 3–4 months. Frontal cortex exposure was generally linear with increasing dose at all time points. Evidence of accumulation was observed in this tissue after multiple doses, with the siRNA exposure after the third monthly 0.3 mg dose equivalent to a single 0.9 mg dose, with additive accumulation observed after the fourth and fifth doses. The dose-exposure relationship of the *Sod1* C16-siRNA could be characterized across all dose levels explored with a first-order pharmacokinetic model.

C16-siRNAs are potent and durable in NHP CNS. To understand whether the C16 and VP siRNA modifications that enable robust CNS activity in the rat would translate to NHPs, we used an amyloid precursor protein (*APP*)-targeting siRNA (Supplementary Table 1). After a single IT dose of 60 mg, siRNA lacking C16 as well as VP had minimal activity in the spinal cord and no activity in the brain at 3 months post-dose (Fig. 3a). Consistent with the rat data, siRNA containing both VP and C16 had the best activity across CNS regions, with up to 70% *APP* knockdown in the spinal

Fig. 1 | Optimization of the siRNA design for CNS delivery in the rat. **a**, 5' *Sod1*-targeting siRNA was conjugated to lipids via 2'-O position at N6 nucleotide of the sense strand and administered as a single IT bolus injection to rats at 0.9 mg (on the basis of siRNA sequence I; Supplementary Table 1). Spinal cord and brain regions were collected 2 weeks post-dose for *Sod1* mRNA knockdown measurement by RT-qPCR. *n* = 4 animals per group. **b**, Single C16 modification walk across sense strand and antisense strand of siRNA and transfected into RPE-J cells for potency assessment via RT-qPCR. *n* = 3 biologically independent samples. **c**, C16 at various positions of *Sod1*-targeting siRNA was evaluated after a single IT bolus injection to rats at 0.9 mg for knockdown in spinal cord and brain regions by RT-qPCR. *n* = 3 animals per group. **d**, Partially or fully modified (ESC, ESC+) 5'-VP-modified *Sod1*-targeting siRNA (Supplementary Table 1) was conjugated to C16 at N6 of the sense strand and administered as a single IT bolus injection to rats at 0.9 mg. Spinal cord and brain regions were collected 2 weeks post-dose for *Sod1* mRNA knockdown measurement by RT-qPCR. *n* = 3 animals per group for aCSF and partially modified; *n* = 5 animals per group for ESC; *n* = 2 animals per group for ESC+. **e**, *Sod1*-targeting siRNA was modified with VP at the 5' end of the antisense strand, with 2'-O-C16 at N6 of the sense strand or with both and administered as a single IT bolus injection to rats at 0.9 mg. Spinal cord, brain regions and peripheral organs were collected at 1 month post-dose for *Sod1* mRNA knockdown measurement by RT-qPCR. *n* = 3 animals per group. All error bars represent standard deviation. **f**, Unconjugated or C16-modified *Sod1*-targeting siRNA was administered as a single IT bolus injection to rats at 0.9 mg, and siRNA biodistribution was assessed in whole brain at 24 h post-dose using IHC with anti-siRNA antibody. Three animals were analyzed per group with similar results.



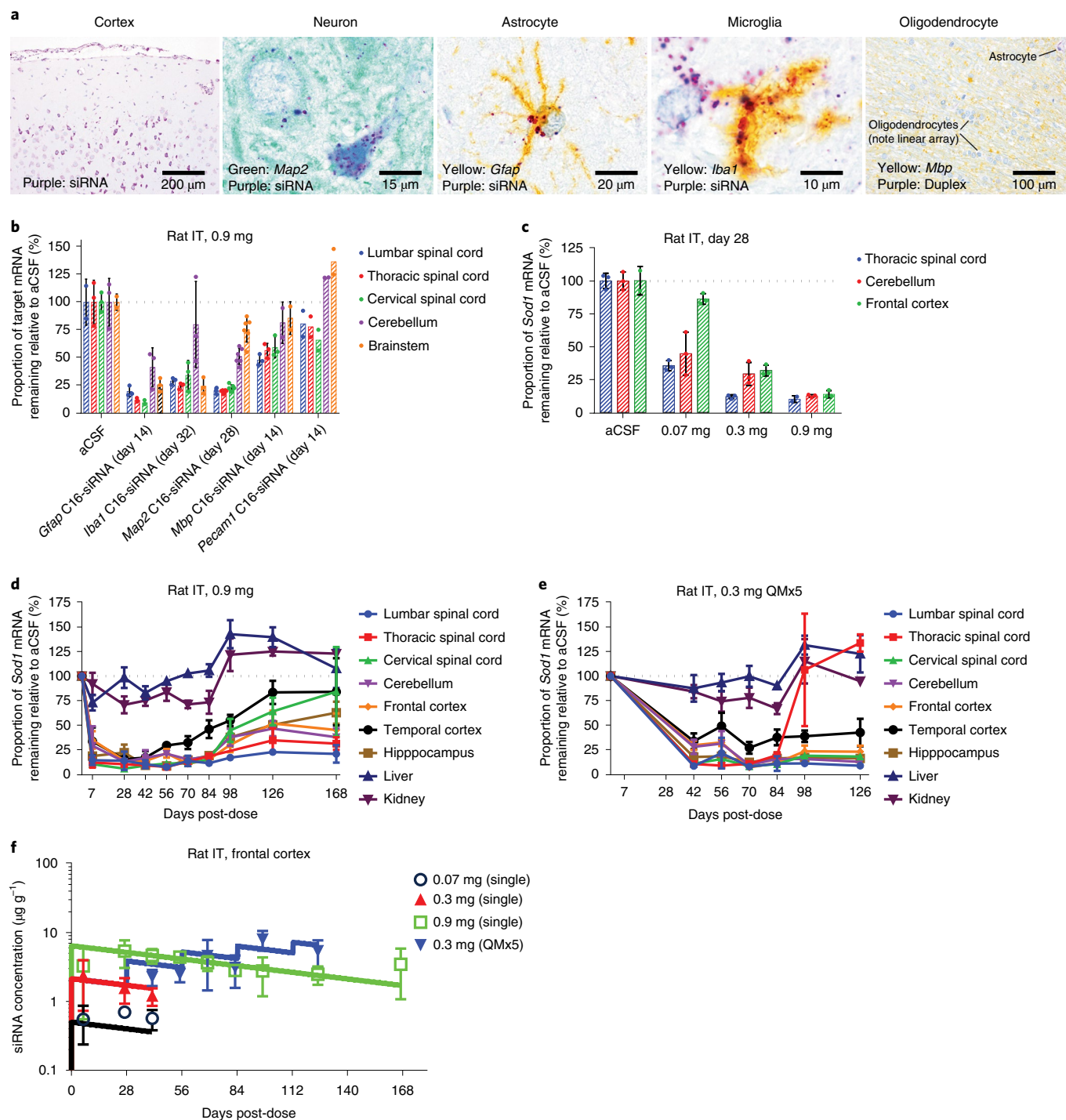


Fig. 2 | Characterization of the C16-siRNA in rat CNS. **a**, siRNA IHC demonstrating robust neuronal and glial cell drug accumulation (magenta) in cerebral cortex (left panel). Dual IHC for the detection of siRNA and cell-type-specific targets in neurons (*Map2*), astrocytes (*Gfap*) and microglia (*Iba1*). siRNA signal in oligodendrocytes (*Mbp*) was below the IHC detection limit. Three animals were analyzed per group with similar results. **b**, C16-siRNAs targeting CNS cell-type-specific transcripts were administered as a single IT bolus injection to rats at 0.9 mg. Spinal cord and brain regions were collected at 2 weeks post-dose (*Gfap*, *Pecam1* and *Mbp*) or 1 month post-dose (*Map2* and *Iba1*) for target mRNA knockdown measurement by RT-qPCR. $n = 3$ animals per group for aCSF, *Gfap*, *Iba1* and *Mbp*; $n = 6$ animals per group for *Map2*; $n = 2$ animals per group for *Pecam1*. **c**, C16-siRNA targeting *Sod1* was administered as a single IT bolus injection to rats at 0.07 mg, 0.3 mg or 0.9 mg. Spinal cord and brain regions were collected at 1 month post-dose for target mRNA knockdown measurement by RT-qPCR. $n = 3$ animals per group. **d**, C16-siRNA targeting *Sod1* was administered as a single IT bolus injection to rats at 0.9 mg. Spinal cord, brain regions and peripheral organs were collected at indicated days post-dose, out to 6 months, for target mRNA knockdown measurement by RT-qPCR. $n = 3$ animals per group. **e**, C16-siRNA targeting *Sod1* was administered as a monthly IT bolus injection to rats at 0.3 mg for a total of up to five injections over 4 months. Spinal cord, brain regions and peripheral organs were collected at indicated days, out to 4.5 months, for target mRNA knockdown measurement by RT-qPCR. $n = 3$ animals per group. **f**, *Sod1* C16-siRNA was administered as single IT injections of 0.07 mg, 0.3 mg or 0.9 mg or monthly 0.3 mg injections for a total of up to five injections over 4 months. Frontal cortex concentrations show dose linearity in the single-dose escalation study in rats and additive exposure in the multi-dose arm. The straightforward pharmacokinetics of C16-siRNA in rat CNS are well-characterized by a first-order pharmacokinetic model (solid lines). $n = 3$ animals per group. All error bars represent standard deviation.

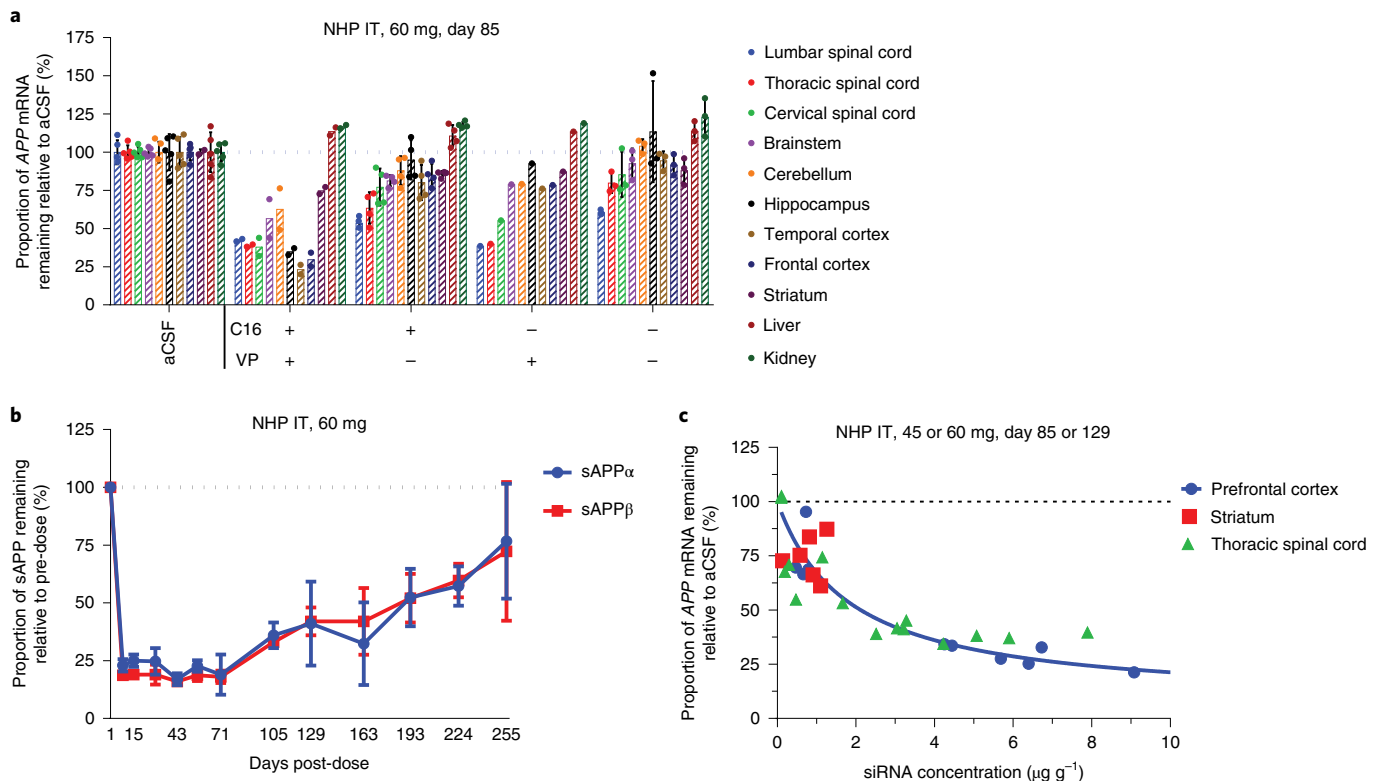


Fig. 3 | Translation of C16-siRNA activity in NHP CNS. **a**, *APP*-targeting siRNA (compounds VII, VIII, IX and X; Supplementary Table 1) was administered as a single IT bolus injection to cynomolgus monkeys at 60 mg, and, 3 months post-dose, tissue samples were analyzed for *APP* mRNA levels by RT-qPCR after 85 days. $n=5$ animals per group for aCSF; $n=2$ animals per group for +VP/+C16; $n=4$ animals per group for -VP/+C16; $n=1$ animal per group for +VP/-C16; $n=3$ animals per group for -VP/-C16. **b**, C16-siRNA targeting *APP* was administered as a single IT bolus injection to three cynomolgus monkeys at 60 mg. CSF was collected at indicated days post-dose, out to 9 months, for sAPP α and sAPP β measurement relative to pre-dose. $n=3$ animals per group. **c**, C16-siRNA concentrations were evaluated by mass spectrometry from CNS tissue samples obtained from animals from **a** and **b** and from a third group of animals ($n=3$) killed at 4.5 months after a 45 mg nominal dose. All error bars represent standard deviation.

cord and up to 80% in the brain, including 25% knockdown in the striatum. There was no activity in NHP liver or kidney at 3 months post-60 mg IT dose.

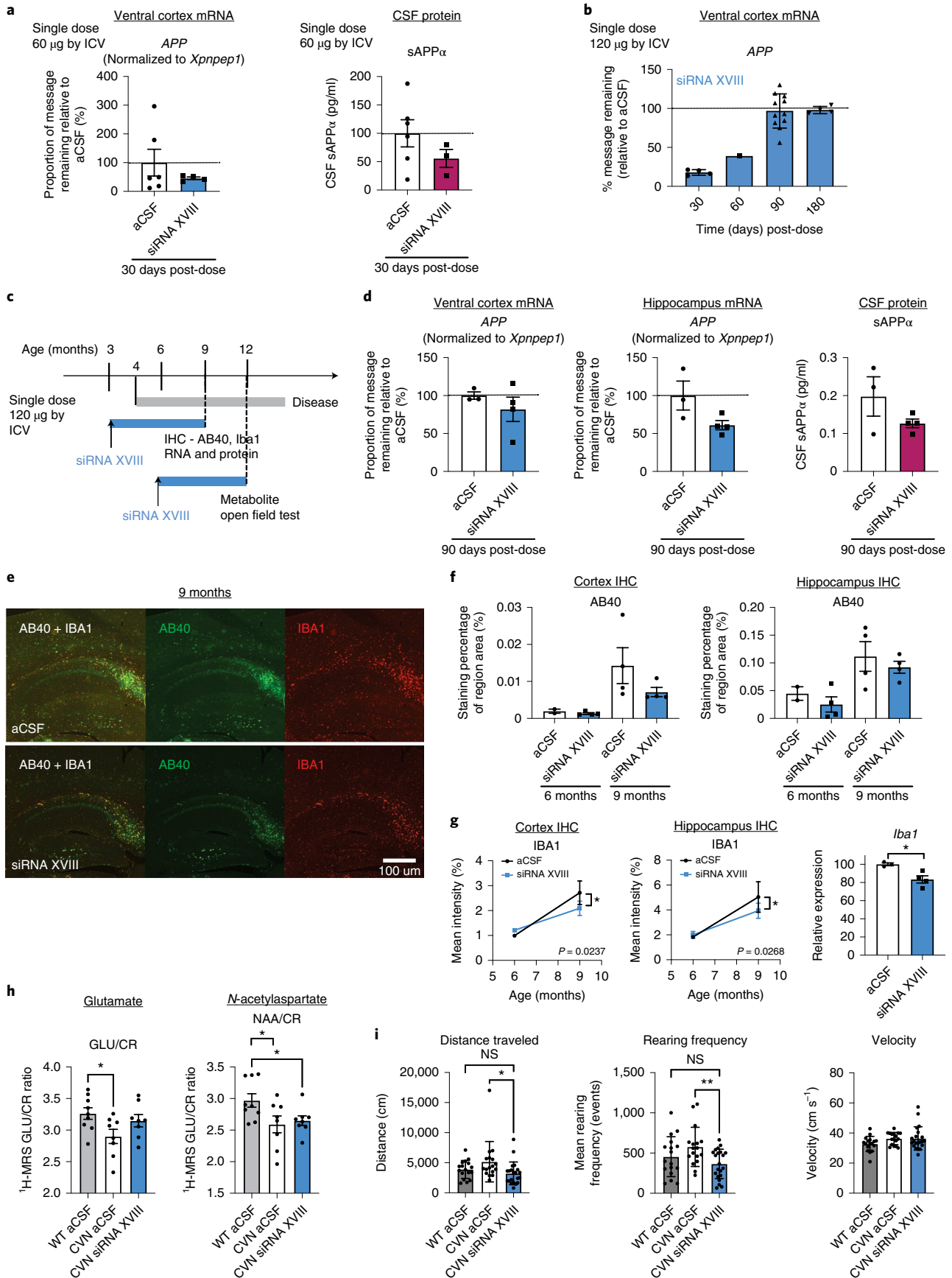
Duration of silencing in the NHPs was evaluated by analyzing serially collected cerebrospinal fluid (CSF) samples using soluble APP α (sAPP α) and soluble APP β (sAPP β) protein biomarker assays (Fig. 3b). Nadir of knockdown was observed at 1 week post-dose (the earliest time point tested), with sustained >75% APP silencing for approximately 2.5 months, 50% at 4.5 months and approaching full recovery at 9 months in most animals.

The relationship of *APP* silencing in CNS tissues to exposure was evaluated in samples from animals in Fig. 3a,b as well as a third cohort of animals that was killed at approximately 4.5 months after

a single 45 mg dose of C16-siRNA. The exposures in the frontal cortex and thoracic spinal cord ranged from <1 $\mu\text{g g}^{-1}$ to approximately 9 $\mu\text{g g}^{-1}$ in these animals (Fig. 3c) and largely reflected the variability in IT administration, as has been previously noted for ASOs²⁶. Fortunately, the variability in dosing allowed us to observe a robust exposure-response relationship across brain regions analyzed.

To evaluate the tolerability and safety in NHPs, histopathological evaluations of brain, spinal cord and dorsal root ganglia were performed after terminal necropsy procedures at 3 months, 6 months or 9 months after a single IT dose of up to 60 mg using the *APP*-targeting siRNAs (Supplementary Table 1). *APP* siRNAs, with or without VP and/or N6 C16 conjugation, were well-tolerated, and there were no test item-related microscopic findings in the

Fig. 4 | Efficacy of *APP* silencing in the CVN mouse model. **a**, Human *APP*-targeting siRNA XVIII (Supplementary Table 1) reduced *APP* mRNA and sAPP α protein. aCSF, $n=6$ per group; siRNA XVIII, $n=3$ per group. **b**, Single 120 μg ICV bolus dose showed ~75% reduction of *APP* mRNA at 30 days and >50% reduction at 60 days post-dose. Day 30 and Day 180, $n=4$ per group; Day 60, $n=1$ per group; Day 90, $n=11$ per group. **c**, Overview of the experimental design and disease progression in the CVN mice. Animals were dosed pre-symptomatically and assessed by IHC for changes in deposition of AB40 (**e,f**) and inflammation (IBA1) (**e,g**) within the cortex and hippocampus 3 months or 6 months post-dose. **d**, After 3 months, a reduction of ~25% and ~50% of *APP* mRNA was observed in the cortex and hippocampus, respectively, which corresponded to a ~50% reduction in sAPP α protein. aCSF, $n=3$ per group; siRNA XVIII, $n=4$ per group. **f**, Tissue AB40 deposits assessed by IHC. aCSF, $n=2$ per group at 6 months; $n=4$ for the remaining groups. **g**, Tissue IBA1 levels assessed by IHC and qPCR (*Iba1*). aCSF, $n=2$ per group at 6 months; $n=4$ for the remaining groups. Simple linear regression was used to compare the slopes. $*P<0.05$ ($P=0.0237$ in the siRNA XVIII group). **h**, Glutamate and *N*-acetylaspartate levels as measured by ¹H-MRS at 12 months of age (6 months post-dose) show normalization of glutamate levels in the siRNA-treated group. WT aCSF, $n=9$ per group; $n=8$ per group for the remaining groups. All error bars represent standard error. $*P<0.05$. Unpaired *t*-test assuming equal variance was used. CR, creatine **i**, siRNA-treated animals show normalization of total distance traveled and rearing frequency. WT aCSF, $n=9$ per group; $n=8$ per group for the remaining groups. All error bars represent standard error. $*P<0.05$, $**P<0.005$. Unpaired *t*-test assuming equal variance was used unless indicated otherwise. NS, not significant.



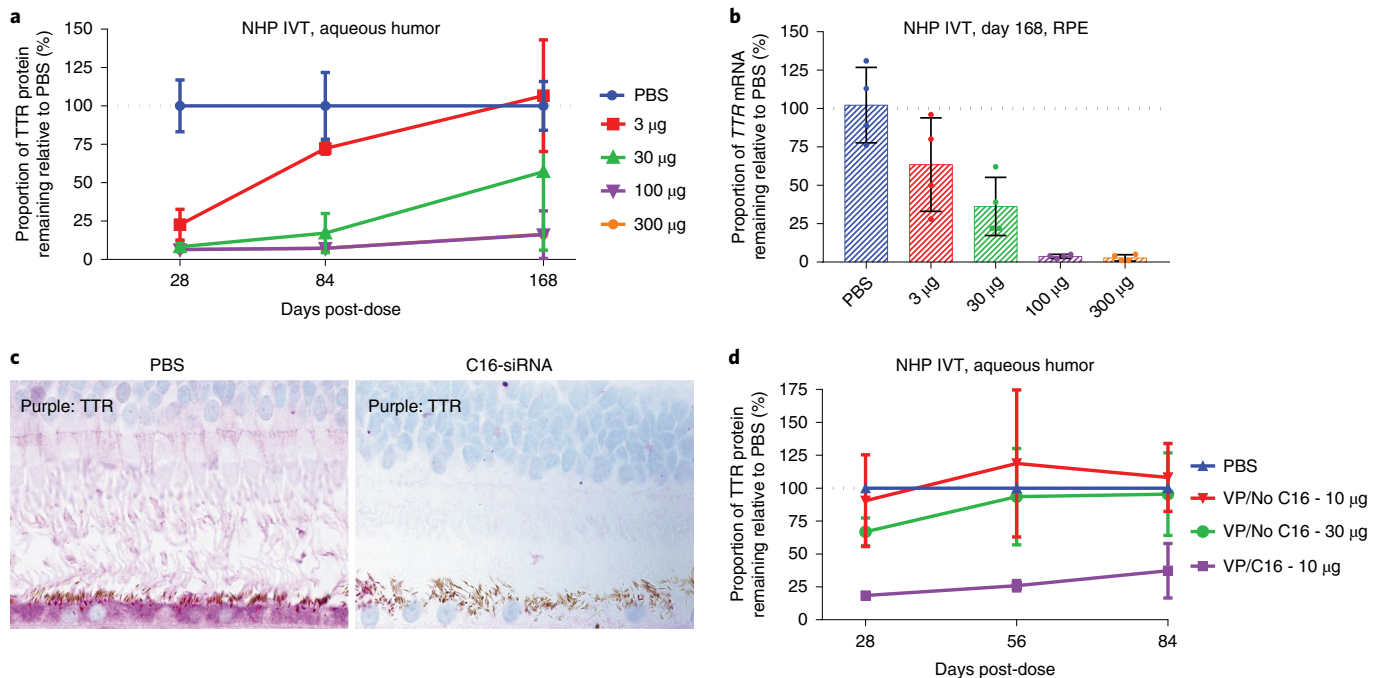


Fig. 5 | Translation of C16-siRNA activity in NHP eye. **a**, C16-siRNA targeting *TTR* (compound XI; Supplementary Table 1) was administered via IVT injection to cynomolgus monkeys at various doses. Aqueous humor was collected for secreted TTR protein measurement relative to PBS-dosed animals. $n = 4$ animals per group. **b**, *TTR* knockdown via RNAi was further confirmed on day 168 by *TTR* mRNA normalized to housekeeping *GAPDH* mRNA relative to PBS-dosed animals in micro-dissected RPE. $n = 4$ animals per group. **c**, TTR IHC confirmed protein knockdown in RPE, along with knockdown of secreted protein adherent to photoreceptor cells above. **d**, Unconjugated *TTR*-targeting siRNA modified with VP at the 5' end of the antisense strand was dosed IVT in cynomolgus monkeys at 10 µg per eye and 30 µg per eye and compared with a dose of 10 µg per eye of the C16-conjugated version. Aqueous humor was collected at indicated days post-dose, out to 3 months, for secreted TTR protein measurement relative to PBS-dosed animals. $n = 4$ animals per group. All error bars represent standard deviation.

examined brain, spinal cord, dorsal root ganglia and liver sections (Extended Data Figs. 1–3). Additionally, conjugation of the C16 ligand to fully chemically modified siRNAs did not induce cytokine release in a human whole blood assay (Supplementary Table 2).

Preclinical efficacy of C16-siRNA in a mouse model of Alzheimer's disease. To evaluate the preclinical efficacy of C16-siRNAs, we used the *Tg-hAPP^{SwDI/mNos2}*^{-/-} (CVN) transgenic mouse expressing human *APP* harboring the Swedish K670N/M671L, Dutch E693Q and Iowa D694N mutations crossed to a *Nos2*^{-/-} background²⁷, which accumulates Aβ in the brain parenchyma and vasculature²⁸. Using an *APP* targeting C16-siRNA, XVIII (Supplementary Table 1), we demonstrated that a single 60 µg ICV administration reduced *APP* mRNA and sAPPα protein levels by 50% in the ventral cortex (VC) and CSF (Fig. 4a). A higher dose at 120 µg showed a ~75% reduction of *APP* mRNA at 30 days and >50% reduction at 60 days, finally normalizing at 90 days in the VC (Fig. 4b,d). When dosed at 3 months of age (Fig. 4c), hippocampal *APP* mRNA and CSF sAPPα protein levels remained reduced at ~40–50% after 90 days (Fig. 4d). We further asked whether knockdown of *APP* is sufficient to reduce pathology in the CVN mice and divided the study into two categories: the first group, dosed pre-symptomatically, was assessed for Aβ40 (AB40) deposits as well as inflammation; the second group, dosed post-symptomatically, was evaluated for changes in metabolites as well as behavior (Fig. 4c). Knockdown of *APP* lasted for 3 months in the VC (Fig. 4b); however, AB40 deposits were reduced by ~50% even after 6 months (Fig. 4e, f), albeit not significantly due to the small sample size ($n = 2–4$). In this model, ionized calcium-binding adaptor molecule 1 (*Iba1*) is upregulated at 4 months and continues to elevate at 9 months, concomitant with increases in inflammation when neurodegeneration occurs²⁹.

The siRNA XVIII-treated group showed a significantly slower rate of increase in IBA1 IHC intensity in the cortex and hippocampus (Fig. 4g). In addition, the expression of *Iba1* mRNA was reduced by 20–30% in siRNA XVIII-treated animals after 6 months (Fig. 4g).

To determine whether decreases in Aβ deposition and inflammation can be associated with restoration of neuronal function, we used proton magnetic resonance spectroscopy³⁰ (¹H-MRS) to measure metabolites, such as glutamate (Glu) and *N*-acetylaspartate (NAA). These metabolites have been found to be reduced in patients with Alzheimer's disease, are reflective of neuronal integrity and are predictors of cognitive deficits^{31,32}. Here, we noted a significant reduction in both Glu and NAA levels in the CVN mice at 12 months of age compared with wild-type (WT) (Fig. 4h). Knockdown of *APP* in the CVN mice normalized Glu levels to that of the WT; however, it had little effect on NAA levels (Fig. 4h). In the open field test, we observed that the CVN mice showed a measurable increase in total distance traveled and an increase in rearing frequency (Fig. 4i). Treatment with siRNA XVIII normalized both measures to levels seen in the WT (Fig. 4i). Velocity measures in all groups were not significantly different from each other (Fig. 4i).

C16 siRNA shows potent and durable activity in the eye. To assess potency and durability in NHP eyes, we used a transthyretin (*TTR*)-targeting C16-siRNA with VP (Supplementary Table 1). A single IVT dose of this conjugate showed dose-dependent lowering of TTR protein in the aqueous humor, with >80% sustained knockdown for 6 months at 100 µg per eye or 300 µg per eye (Fig. 5a). In the retinal pigmented epithelium (RPE), dose-dependent *TTR* mRNA lowering was observed, with >95% knockdown at a dose of 100 µg per eye (Fig. 5b). TTR protein knockdown in RPE cells was further confirmed by TTR IHC at 6 months post-dose (Fig. 5c).

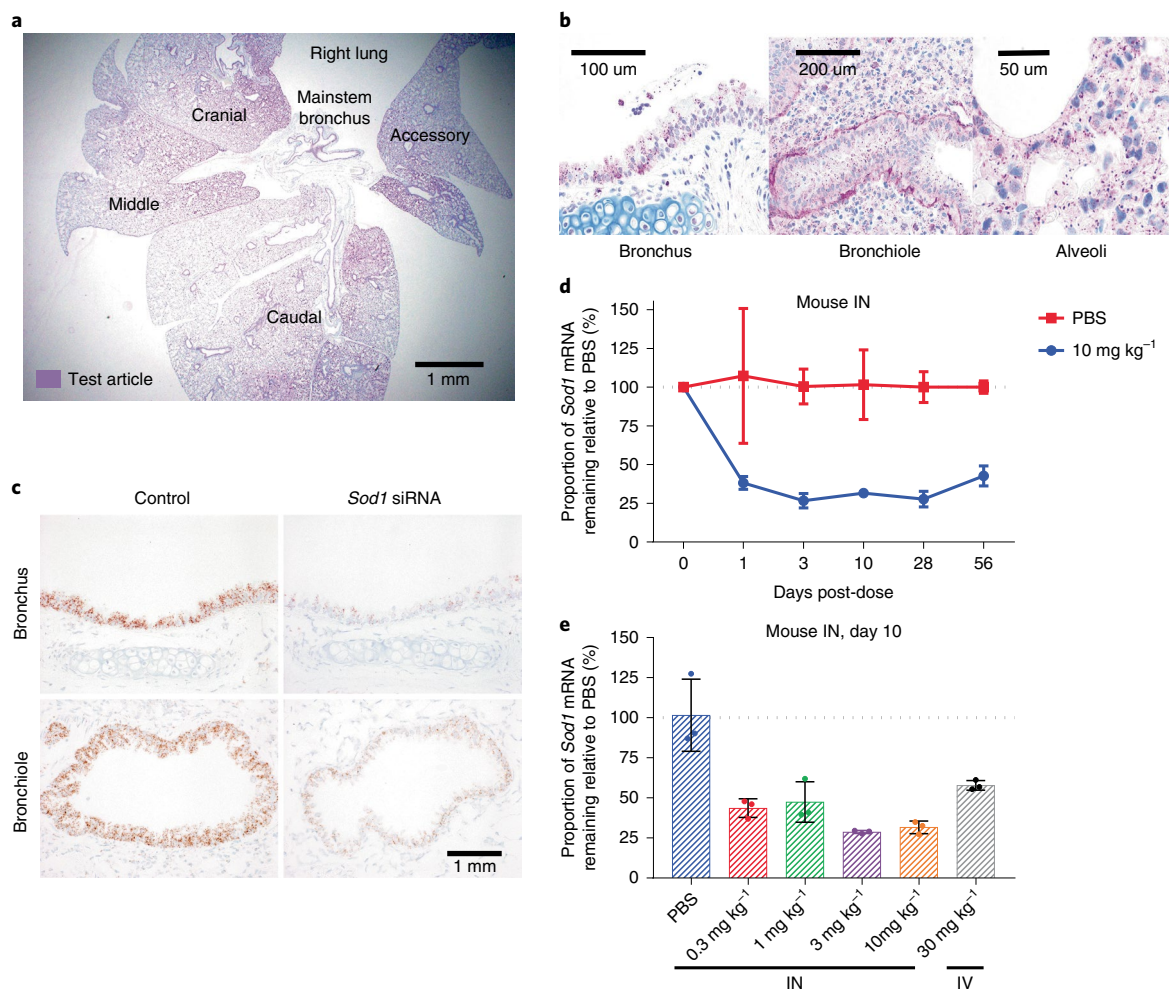


Fig. 6 | C16-siRNA distribution and activity in mouse lung. **a, b**, C16-siRNAs were administered in mice intranasally at 10 mg kg⁻¹ (*Sod1*) (**a**) or 30 mg kg⁻¹ (*Traf6*) (**b**) (Supplementary Table 1). Lungs were collected on day 10 or day 28 post-dose, respectively, for siRNA IHC. siRNA, magenta; hematoxylin counterstain, blue. Three animals were analyzed per group with similar results. **c**, *Sod1* mRNA knockdown was visualized by ISH on day 10 after 10 mg kg⁻¹ IN dose of *Sod1*-targeting C16-siRNA. *Sod1* mRNA, brown; hematoxylin counterstain, blue. Three animals were analyzed per group with similar results. **d**, RT-qPCR of *Sod1* mRNA in whole lung measured on day 10 after 0.3, 1, 3 or 10 mg kg⁻¹ single IN dose or 30 mg kg⁻¹ single IV dose of *Sod1*-targeting C16-siRNA. *n* = 3 animals per group. All error bars represent standard deviation. **e**, RT-qPCR of *Sod1* mRNA in whole lung measured at multiple time points after 10 mg kg⁻¹ IN dose of *Sod1*-targeting C16-siRNA. *n* = 3 animals per group.

The unconjugated siRNAs (without C16) showed no knockdown at a dose of 10 μg per eye and a modest 33% knockdown at a dose of 30 μg per eye compared with 81% knockdown observed for the C16 conjugate at a dose of 10 μg per eye (Fig. 5d).

C16 siRNA shows potent and durable siRNA activity in the lung. C16-siRNA distribution in the mouse lung tissue was evaluated after intranasal (IN) administration using IHC (Fig. 6a,b and Supplementary Table 1). siRNA distributed throughout the whole lung, with the greatest accumulation near the mainstem bronchi (Fig. 6a). Closer evaluation showed robust bronchiolar and alveolar uptake (Fig. 6b). The siRNA distribution correlated well with RNAi activity assessed by in situ hybridization (ISH) of the *Sod1* mRNA (Fig. 6c). We were not able to assess activity in the alveoli because *Sod1* is expressed only in the large airways. The RNAi activity was dose dependent as measured by *Sod1* mRNA from whole lung tissue (Fig. 6e) and was sustained out to 2 months post-dose, with 57% mRNA lowering at 10 mg kg⁻¹ via IN administration (Fig. 6d). The single intravenous (IV) injection at 30 mg kg⁻¹ reduced *Sod1* mRNA by 42% (Fig. 6e), indicating a clear benefit of IN administration for delivery of C16-siRNAs to the lungs.

Discussion

Systematic efforts to optimize RNAi therapeutics for potent, durable and safe silencing of disease-associated gene transcripts in the liver^{9,10,33} provided the framework for designing siRNAs for extrahepatic applications. Lipophilic ligands, primarily cholesterol, conjugated via a linker to the 5' or 3' ends of the siRNA, have been widely used to facilitate systemic and local siRNA delivery into extrahepatic tissues^{23,34–37}, including the eye³⁸, lung³⁵ and CNS^{21,39,40}, albeit with limited distribution beyond the injection site and, in certain cases, an unacceptable safety profile⁴¹. Here we report, to our knowledge for the first time, a systematic evaluation of lipophilic siRNA conjugates combined with additional design features to arrive at an optimal conjugate design that enables widespread siRNA distribution in the spinal cord and brain after administration into rodents and NHPs via a clinically feasible IT dosing route, with a favorable safety profile. Notably, we provide a preclinical proof-of-concept study whereby administration of a C16-siRNA targeting *APP* in a mouse model of Alzheimer's disease produced a sufficiently potent and durable knockdown in the CNS to both alter the physiological deficits, such as Aβ deposition and inflammation, and normalize behavioral deficits. This program has already advanced into clinical

development for the treatment of early onset Alzheimer's disease and cerebral amyloid angiopathy.

The same C16 conjugation strategy also enables broad siRNA distribution and durable activity in the eye and lung after local delivery. Combined with the durability of siRNAs, the addition of the C16 conjugation has the potential for therapeutic silencing of target genes outside the liver with infrequent dosing. The precise mechanisms whereby C16 promotes intracellular delivery is currently under investigation; however, we hypothesize that it promotes moderate affinity interactions with the extracellular matrix and various cell membrane components, thus allowing for binding and uptake into various cell types.

Online content

Any methods, additional references, Nature Research reporting summaries, source data, extended data, supplementary information, acknowledgements, peer review information; details of author contributions and competing interests; and statements of data and code availability are available at <https://doi.org/10.1038/s41587-022-01334-x>.

Received: 28 September 2021; Accepted: 22 April 2022;

Published online: 2 June 2022

References

- Setten, R. L., Rossi, J. J. & Han, S. P. The current state and future directions of RNAi-based therapeutics. *Nat. Rev. Drug Discov.* **18**, 421–446 (2019).
- Adams, D. et al. Patisiran, an RNAi therapeutic, for hereditary transthyretin amyloidosis. *N. Engl. J. Med.* **379**, 11–21 (2018).
- Kristen, A. V. et al. Patisiran, an RNAi therapeutic for the treatment of hereditary transthyretin-mediated amyloidosis. *Neurodegener. Dis. Manag.* **9**, 5–23 (2019).
- Balwani, M. et al. Phase 3 trial of RNAi therapeutic givosiran for acute intermittent porphyria. *N. Engl. J. Med.* **382**, 2289–2301 (2020).
- Garrelfs, S. F. et al. Lumasiran, an RNAi therapeutic for primary hyperoxaluria type 1. *N. Engl. J. Med.* **384**, 1216–1226 (2021).
- Raal, F. J. et al. Inclisiran for the treatment of heterozygous familial hypercholesterolemia. *N. Engl. J. Med.* **382**, 1520–1530 (2020).
- Ray, K. K. et al. Inclisiran in patients at high cardiovascular risk with elevated LDL cholesterol. *N. Engl. J. Med.* **376**, 1430–1440 (2017).
- Ray, K. K. et al. Two phase 3 trials of inclisiran in patients with elevated LDL cholesterol. *N. Engl. J. Med.* **382**, 1507–1519 (2020).
- Foster, D. J. et al. Advanced siRNA designs further improve in vivo performance of GalNAc-siRNA conjugates. *Mol. Ther.* **26**, 708–717 (2018).
- Janas, M. M. et al. Selection of GalNAc-conjugated siRNAs with limited off-target-driven rat hepatotoxicity. *Nat. Commun.* **9**, 723 (2018).
- Nair, J. K. et al. Impact of enhanced metabolic stability on pharmacokinetics and pharmacodynamics of GalNAc-siRNA conjugates. *Nucleic Acids Res.* **45**, 10969–10977 (2017).
- Nair, J. K. et al. Multivalent N-acetylgalactosamine-conjugated siRNA localizes in hepatocytes and elicits robust RNAi-mediated gene silencing. *J. Am. Chem. Soc.* **136**, 16958–16961 (2014).
- Alterman, J. F. et al. A divalent siRNA chemical scaffold for potent and sustained modulation of gene expression throughout the central nervous system. *Nat. Biotechnol.* **37**, 884–894 (2019).
- Zhou, Y. et al. Blood-brain barrier-penetrating siRNA nanomedicine for Alzheimer's disease therapy. *Sci. Adv.* **6**, eabc7031 (2020).
- Gregory, J. V. et al. Systemic brain tumor delivery of synthetic protein nanoparticles for glioblastoma therapy. *Nat. Commun.* **11**, 5687 (2020).
- Eyford, B. A. et al. A nanomule peptide carrier delivers siRNA across the intact blood-brain barrier to attenuate ischemic stroke. *Front. Mol. Biosci.* **8**, 611367 (2021).
- Nagata, T. et al. Cholesterol-functionalized DNA/RNA heteroduplexes cross the blood-brain barrier and knock down genes in the rodent CNS. *Nat. Biotechnol.* **39**, 1529–1536 (2021).
- Gupta, A., Kafetzis, K. N., Tagalakis, A. D. & Yu-Wai-Man, C. RNA therapeutics in ophthalmology—translation to clinical trials. *Exp. Eye Res.* **205**, 108482 (2021).
- DeVincenzo, J. et al. A randomized, double-blind, placebo-controlled study of an RNAi-based therapy directed against respiratory syncytial virus. *Proc. Natl Acad. Sci. USA* **107**, 8800–8805 (2010).
- Chappell, A. E. et al. Mechanisms of palmitic acid-conjugated antisense oligonucleotide distribution in mice. *Nucleic Acids Res.* **48**, 4382–4395 (2020).
- Chen, Q. et al. Lipophilic siRNAs mediate efficient gene silencing in oligodendrocytes with direct CNS delivery. *J. Control. Release* **144**, 227–232 (2010).
- Manoharan, M. Oligonucleotide conjugates as potential antisense drugs with improved uptake, biodistribution, targeted delivery, and mechanism of action. *Antisense Nucleic Acid Drug Dev.* **12**, 103–128 (2002).
- Wolfgram, C. et al. Mechanisms and optimization of in vivo delivery of lipophilic siRNAs. *Nat. Biotechnol.* **25**, 1149–1157 (2007).
- Schlegel, M. K. et al. Chirality dependent potency enhancement and structural impact of glycol nucleic acid modification on siRNA. *J. Am. Chem. Soc.* **139**, 8537–8546 (2017).
- Parmar, R. et al. 5'-(E)-vinylphosphonate: a stable phosphate mimic can improve the RNAi activity of siRNA-GalNAc conjugates. *ChemBioChem* **17**, 985–989 (2016).
- Sullivan, J. M. et al. Convective forces increase rostral delivery of intrathecal radiotracers and antisense oligonucleotides in the cynomolgus monkey nervous system. *J. Transl. Med.* **18**, 309 (2020).
- Wilcock, D. M. et al. Progression of amyloid pathology to Alzheimer's disease pathology in an amyloid precursor protein transgenic mouse model by removal of nitric oxide synthase 2. *J. Neurosci.* **28**, 1537–1545 (2008).
- Colton, C. A. et al. *mNos2* deletion and human *NOS2* replacement in Alzheimer disease models. *J. Neuropathol. Exp. Neurol.* **73**, 752–769 (2014).
- Kan, M. J. et al. Arginine deprivation and immune suppression in a mouse model of Alzheimer's disease. *J. Neurosci.* **35**, 5969–5982 (2015).
- Hall, H. et al. Magnetic resonance spectroscopic methods for the assessment of metabolic functions in the diseased brain. *Curr. Top. Behav. Neurosci.* **11**, 169–198 (2012).
- Su, L. et al. Whole-brain patterns of ¹H-magnetic resonance spectroscopy imaging in Alzheimer's disease and dementia with Lewy bodies. *Transl. Psychiatry* **6**, e877 (2016).
- Wang, H. et al. Magnetic resonance spectroscopy in Alzheimer's disease: systematic review and meta-analysis. *J. Alzheimers Dis.* **46**, 1049–1070 (2015).
- Janas, M. M. et al. Safety evaluation of 2'-deoxy-2'-fluoro nucleotides in GalNAc-siRNA conjugates. *Nucleic Acids Res.* **47**, 3306–3320 (2019).
- Osborn, M. F. & Khvorova, A. Improving siRNA delivery in vivo through lipid conjugation. *Nucleic Acid Ther.* **28**, 128–136 (2018).
- Biscans, A. et al. Diverse lipid conjugates for functional extra-hepatic siRNA delivery in vivo. *Nucleic Acids Res.* **47**, 1082–1096 (2019).
- Raouane, M., Desmae, D., Urbinati, G., Massaad-Massade, L. & Couvreur, P. Lipid conjugated oligonucleotides: a useful strategy for delivery. *Bioconjug. Chem.* **23**, 1091–1104 (2012).
- Kubo, T. et al. Palmitic acid-conjugated 21-nucleotide siRNA enhances gene-silencing activity. *Mol. Pharm.* **8**, 2193–2203 (2011).
- Byrne, M. et al. Novel hydrophobically modified asymmetric RNAi compounds (sd-rxRNA) demonstrate robust efficacy in the eye. *J. Ocul. Pharmacol. Ther.* **29**, 855–864 (2013).
- DiFiglia, M. et al. Therapeutic silencing of mutant huntingtin with siRNA attenuates striatal and cortical neuropathology and behavioral deficits. *Proc. Natl Acad. Sci. USA* **104**, 17204–17209 (2007).
- Alterman, J. F. et al. Hydrophobically modified siRNAs silence Huntingtin mRNA in primary neurons and mouse brain. *Mol. Ther. Nucleic Acids* **4**, e266 (2015).
- Nikan, M. et al. Docosahexaenoic acid conjugation enhances distribution and safety of siRNA upon local administration in mouse brain. *Mol. Ther. Nucleic Acids* **5**, e344 (2016).

Publisher's note Springer Nature remains neutral with regard to jurisdictional claims in published maps and institutional affiliations.

© The Author(s), under exclusive licence to Springer Nature America, Inc. 2022

Methods

Care and use of laboratory animals. All studies were conducted using protocols consistent with local, state and federal regulations, as applicable, and approved by the Institutional Animal Care and Use Committees (IACUCs) at Alnylam Pharmaceuticals, Charles River Laboratories (CRL) or LabCorp (formerly Covance) as applicable. Animal studies in Figs. 1a,d,e and 2b were conducted in 8–10-week-old female Sprague Dawley rats and approved by the IACUC at Alnylam Pharmaceuticals. Animal studies in Figs. 1c,f and 2c–f were conducted in 8–10-week-old male Sprague Dawley rats and approved by the IACUC at CRL (Figs. 1c and 2c–f) or Alnylam Pharmaceuticals (Fig. 1f). Animal studies in Fig. 4 and in Extended Data figures were conducted in 2–4-year-old male cynomolgus macaques and approved by the IACUC at CRL. Animal studies in Fig. 5 were conducted in 2–5-year-old female cynomolgus macaques and approved by the IACUC at CRL. Animal studies in Fig. 5 were conducted in 8–10-week-old female C57BL/6 mice and approved by the IACUC at Alnylam Pharmaceuticals. Animal numbers are provided in figure legends.

Oligonucleotide synthesis. All oligonucleotides were synthesized on an MerMade 192 or MerMade 12 synthesizer according to previously published protocols^{34,42}. 5'-O-(4,4'-dimethoxytrityl)-2'-deoxy-2'-fluoro- and 5'-O-(4,4'-dimethoxytrityl)-2'-O-methyl-3'-O-(2-cyanoethyl-N,N-diisopropyl) phosphoramidite monomers of uridine, 4-N-acetylcytidine, 6-N-benzoyladenine and 2-N-isobutylguanosine were purchased commercially, and (S)-GNA phosphoramidites were synthesized according to previously published protocols^{43–45}. 2'-O-C16 phosphoramidites (WO2019217459) were used at a concentration of 100–150 mM in acetonitrile with no other changes to synthetic protocols. Phosphorothioate linkages were introduced by sulfuration of phosphite linkages using 0.1 M 3-(N,N-dimethylaminomethylidene)amino-3H-1,2,4-dithiazole-5-thione (DDTT) in pyridine. After completion of the solid-phase synthesis, the solid support was incubated in a sealed container with aqueous ammonium hydroxide (28–30%) with added 5% diethylamine by volume, with shaking overnight at 35 °C, after a procedure optimized for 5'-(E)-vinyl phosphonate oligonucleotide deprotection⁴⁶. The oligonucleotide was filtered to remove the support with 5× volume of water and analyzed by liquid chromatography–mass spectrometry (LC-MS) and ion exchange (IEX) high-performance liquid chromatography (HPLC).

After de-protection and crude quality confirmation, IEX HPLC purification was performed. Purification buffer A consisted of 20 mM sodium phosphate and 15% acetonitrile, pH 8.5. Buffer B was the same composition with an additional 1 M sodium bromide. TSKgel Super Q-5PW (20) IEX resin (Tosoh, 0018546) was used for purification, and a general purification gradient of 15% to 48% in about 20 column volumes was applied. Fractions were analyzed by IEX analysis using a Dionex DNAPac PA200 IEX analytical column, 4 mm × 250 mm (Thermo Fisher Scientific, 063000) at room temperature. Buffer A consisted of 20 mM sodium phosphate and 15% acetonitrile, pH 12. Buffer B was identical with an additional 1 M sodium bromide. A gradient of 30% to 50% over 12 minutes with a flow rate of 1 ml min⁻¹ was used to analyze fractions. Fractions with >85% purity were pooled, concentrated and desalted over size exclusion columns (GE Healthcare, 17-5087-01) with a flow rate of 10 ml min⁻¹. All oligonucleotides were purified and desalted and further annealed to form siRNA duplexes as previously described¹². All siRNAs were synthesized by Alnylam Pharmaceuticals.

The identities and purities of all oligonucleotides were confirmed using electrospray ionization (ESI)-LC-MS and IEX HPLC, respectively.

In vitro screening. Rat RPE-J cells (American Type Culture Collection, CRL-2240) were transfected by adding 0.1 µl of RNAiMAX (Invitrogen, 13778) diluted in 4.9 µl of Opti-MEM to 5 µl of siRNA in a 384-well plate. After a 15-minute room temperature incubation, 40 µl of media containing ~5 × 10³ cells was added to the wells. Cells were incubated for 24 h, and RNA was isolated using an automated protocol on a BioTek EL406 platform using Dynabeads mRNA DIRECT Purification Kit (Invitrogen, 61012) according to the manufacturer's instructions. RNA was eluted with 150 µl of elution buffer.

Complementary DNA (cDNA) synthesis was performed using High-Capacity cDNA Reverse Transcription Kit (Applied Biosystems, 4368813) according to the manufacturer's instructions. Next, 2 µl of cDNA was added to a master mix containing 0.5 µl of rat *Gapdh* TaqMan probe (Thermo Fisher Scientific, 4352338E), 0.5 µl of rat *Sod1* TaqMan probe (Thermo Fisher Scientific, Rn00566938_m1) and 5 µl of LightCycler 480 probe master mix (Roche, 04887301001) per well in a 384-well plate (Roche, 04887301001). Quantitative PCR with reverse transcription (RT-qPCR) was performed in a LightCycler 480 Real Time PCR system (Roche). qPCR data were analyzed using the ΔΔCt method.

Rat IT studies. siRNAs formulated at up to 30 mg ml⁻¹ in artificial cerebrospinal fluid (aCSF) were administered as 30-µl IT injections by lumbar puncture in the dorsal region of the spine between the L3–L5 vertebral space to male Sprague Dawley rats. At a minimum of 30 minutes before surgery, rats were subcutaneously administered 1 mg kg⁻¹ of meloxicam and 0.1 mg kg⁻¹ of buprenorphine. After anesthesia with isoflurane, rats were placed on a warm heating pad and treated with eye lubricant; the IT injection site was shaved and disinfected; and an incision was made to expose the spinal column. siRNA was administered with an insulin

syringe. Proper placement of the needle was confirmed via CSF backflow in the hub of the needle. Once siRNA administration was completed, gentle constant pressure on the plunger was maintained for 30 seconds; the incision was sutured and secured with tissue glue; and the rats were placed in sternal recumbency on a heating pad until recovery.

NHP IT studies. siRNAs formulated at 30 mg ml⁻¹ in aCSF were administered as 2-ml IT injections over 3 minutes by lumbar puncture in the dorsal region of the spine between the L2–L3, L3–L4, L4–L5 or L5–L6 vertebral space of cynomolgus monkeys. Anesthesia was induced with dexmedetomidine and ketamine and was maintained with supplemental isoflurane as needed. Proper placement of the needle was confirmed via CSF backflow in the hub of the needle. A total volume of 1 ml of CSF was removed before dosing, and 0.3-ml aCSF flush was performed after siRNA administration. After completion of the flush, the syringe and needle were removed; pressure was applied to the injection site for at least 30 seconds; and the animals were allowed to recover. Dexmedetomidine was reversed with atipamezole as necessary. Serial CSF collections were performed from cisterna magna after procedural anesthesia induced with dexmedetomidine and ketamine and maintained with supplemental isoflurane as needed.

NHP IVT studies. A topical antibiotic (tobramycin) was applied to both eyes twice on the day before and twice on the day after IVT injection to cynomolgus monkeys. The animals received an intramuscular injection of a sedative cocktail (ketamine 5 mg kg⁻¹; dexmedetomidine 0.01 mg kg⁻¹) followed by isoflurane/oxygen mix through a mask, if deemed necessary to maintain anesthesia. Either 1× PBS or siRNA formulated in 1× PBS was administered in both eyes by IVT injection using a 1-ml syringe and a 30-gauge, ½-inch needle. The dose volume administered was 50 µl per eye. IVT injections were performed by a board-certified veterinary ophthalmologist. After completion of the dosing procedure, animals received an intramuscular injection of 0.1 mg kg⁻¹ of atipamezole, a reversal agent for dexmedetomidine, as considered necessary. The conjunctivae were flushed with diluted benzalkonium chloride (Zephiran). Mydriatic drops were applied to each eye as needed.

Mouse IN studies. Female C57BL/6 mice (8–10 weeks of age) were dosed via IN instillation (50 µl total, 25 µl per nostril) at the indicated siRNA concentration diluted in 1× PBS and were killed at the indicated day.

CVN mouse studies. Male and female CVN mice were bred at CRL Germany and genotyped, housed, dosed and analyzed (IHC, ¹H-MRS and open field test) at CRL Finland, as previously reported, under regular temperature, humidity and light/dark cycle conditions^{27,28,47}. Homozygous *Tg-hAPP^{SwDI}/mNos2^{-/-}* (CVN) mice were produced by crossing mice expressing the vasculotropic Swedish K670N/M671L, Dutch E693Q and Iowa D694N human *APP* mutations under control of the *Thy-1* promoter⁴⁸ with *mNos2^{-/-}* (B6 129PNos2 tau1Lau/J) mice⁴⁹. The study was divided into two phases. In the first phase, 15 CVN mice were dosed by ICV at 3 months of age, with terminal tissue sampling at 6 months of age and 9 months of age. In the second phase, 40 CVN mice and 20 WT mice were divided into three experimental groups, with terminal tissue sampling at 9 months of age and 12 months of age. Metabolic analyses using ¹H-MRS were at 12 months of age, respectively, as previously described²⁸. Open field test measurements were performed at ~9 months of age. Activity chambers (Med Associates, 27 × 27 × 20.3 cm) were equipped with infrared beams. Mice were placed in the center of the chamber, and their behaviors were recorded for 30 minutes. The following parameters were recorded and analyzed: distance traveled, number of vertical rearings and average velocity. IHC was performed as described^{27,29} using anti-amyloid-beta antibody WO2 (Sigma-Aldrich, MABN10, lot 3557956, 1:500) and anti-IBA1 antibody (Wako Pure Chemicals, 01-1941, lot LEP3218, 1:200). All data are presented as mean ± standard deviation or standard error of the mean, and differences were statistically significant at the *P* < 0.05 level. Statistical analyses were performed using the PRISM statistical program (GraphPad Software).

Mouse ICV infusion. ICV administration was performed using stereotactically guided Hamilton syringe and infusion system (Harvard Apparatus). A single 5-µl unilateral injection was performed in the right lateral ventricle at the following coordinates: AP = -0.5 mm (posterior from bregma), ML = +1.0 mm and DV = -1.75 mm, using standard aseptic surgical procedures. After midline skin incision on the scalp, a burr hole was generated at selected coordinates using stereotaxic coordinates and a dental drill. Thereafter, a small puncture in the dura was made at the epicenter of the burr hole, and the needle was lowered to specified depth to reach the lateral ventricle. A Hamilton syringe with a 28-gauge blunt needle was filled with a volume slightly greater than 5 µl. Administration volume of the test articles was at 5 µl and infusion rate at 1 µl min⁻¹ (over 5 minutes). After the infusion, the needle was left in place for a stabilization period of 5 minutes before withdrawal from the ventricle. Withdrawal is performed slowly and paused for 30 seconds when the needle tip is at the cortical area.

RNA extraction and RT-qPCR. For the extraction of RNA, powdered tissues (~10 mg) were resuspended in 700 µl of QIAzol and homogenized by vigorous pipetting. Alternatively, two 5-mm steel grinding balls were added to each sample,

followed by homogenization at 25 per second for 1 minute at 4 °C using TissueLyser II (Qiagen, 85300). Samples were incubated at room temperature for 5 minutes, followed by the addition of 140 µl of chloroform. Samples were mixed by shaking, followed by a 10-minute incubation at room temperature. Samples were spun at 6,000g for 15 minutes at 4 °C; the supernatant was transferred to a new tube; and 1.5 volumes of 100% ethanol was added. Samples were then purified using an miRNeasy Kit (Qiagen, 217061) according to the manufacturer's instructions. The RNA was eluted from miRNeasy columns with 50–60 µl of RNase-free water and quantified on a NanoDrop (Thermo Fisher Scientific).

cDNA synthesis was performed using High-Capacity cDNA Reverse Transcription Kit (Applied Biosystems, 4368813) according to the manufacturer's instructions. qPCR reactions were performed using gene-specific TaqMan assays for rat *Sod1* (Thermo Fisher Scientific, Rn00566938_m1), rat *Ppib* (Thermo Fisher Scientific, Rn03302274_m1), mouse *Sod1* (Integrated DNA Technologies, Mm.PT.58.12368303), mouse *Gapdh* (Thermo Fisher Scientific, Mm99999915_g1), NHP *APP* (Thermo Fisher Scientific, Mf01552283_m1), NHP *TTR* (Thermo Fisher Scientific, Mf02799963_m1), NHP *PPIB* (Thermo Fisher Scientific, Mf02802985_m1) or NHP *GAPDH* (forward primer: 5'-GCATCCTGGGCTACAC TGA-3', reverse primer: 5'-TGGGTGCTCGTGTGAAGTC-3', probe: 5'-HEX-CC AGGTGCTCTCCTCC-3'-BHQ-1), mouse *Iba1* (Thermo Fisher Scientific, Mm00479862), mouse *Xpnp1* (Thermo Fisher Scientific, Mm00460029) and human *APP* (Thermo Fisher Scientific, Hs00169098). qPCR reactions were performed in a Roche LightCycler 480 using LightCycler 480 Probes Master Mix (Roche, 04707494001). qPCR data were analyzed using the $\Delta\Delta C_t$ method.

Protein analyses. For sAPP protein analysis in NHP CSF, a V-PLEX panel for sAPP α and sAPP β (Meso Scale Discovery, K15120E) was used according to the manufacturer's instructions. Plates were incubated at room temperature for ~10 minutes before reading on a MSD SECTOR Imager Instrument (Meso Scale Discovery).

For TTR protein analysis in NHP aqueous humor, an in-house sandwich ELISA was developed. Then, 96-well Nunc MaxiSorp plates (Invitrogen, 44-2404-21) were coated overnight at 4 °C with rabbit anti-human TTR pAb (Dako, A0002) at a final concentration of 5.63 µg ml⁻¹ prepared in 50 mM carbonate/bicarbonate buffer. The next day, plates were washed 5× with 300 µl of Tris buffer containing 0.05% Tween 20 (TBS-T) on a BioTek plate washer. Plates were blocked with 150 µl per well of 1× Power Block (Biogenex Laboratories, HK0855K) for 2 h at room temperature and washed 5× with 300 µl of TBS-T. An in-house cynomolgus TTR standard was used to prepare the highest standard at 59.5 ng ml⁻¹, followed by a 2.5-fold dilution series in 1× Power Block to generate an 8-point standard curve. Aqueous humor samples were tested at a 1:600 dilution in 1× Power Block. Standards and samples were added to the plate, 100 µl per well, in duplicate and incubated for 2 h at room temperature with shaking at 600 r.p.m. Plates were washed 5× with 300 µl of TBS-T, followed by the addition of secondary antibody, anti-hTTR pAb (Abcam, ab9015), at a final concentration of 4 µg ml⁻¹ prepared in 1× Power Block. Plates were incubated for 1 hour at room temperature with shaking at 600 r.p.m. Plates were washed 5× with 300 µl of TBS-T, and the detection antibody, donkey anti-sheep pAb alkaline phosphatase, was applied at a final concentration of 1.4 µg ml⁻¹ in 1× Power Block (Sigma-Aldrich, A5187). Plates were incubated for 1 hour at room temperature with shaking at 600 r.p.m. Plates were washed 5× with 300 µl of TBS-T, followed by the addition of substrate, 1.0 mg ml⁻¹ of pNPP (Sigma-Aldrich, N2770). Plates were incubated in the dark at room temperature for ~20 minutes before the addition of 1 M sodium hydroxide to stop the reaction. Absorbance was read at 405 nm on an M5 SpectraMax (Molecular Devices). For data analysis, the blank optical density (OD) units were subtracted from all wells, and the OD units for each calibrator were plotted against the calibrator concentrations and fit with a 4-parameter logistical fit. The concentrations of each replicate of unknowns and the back-calculated concentrations of the standards were interpolated to determine the ng ml⁻¹ of TTR.

Quantitation of siRNA. Quantitation of siRNAs was performed by liquid chromatography coupled with high-resolution mass spectrometry (LC-HRMS) as described previously^{50,51}. The samples extracted using a Clarity OTX 96-well plate (Phenomenex) were analyzed by LC-HRMS. The mobile phases used were as follows: mobile phase A: H₂O/HFIP/DIEA (100:1:0.1, v:v:v) with 10 µM EDTA; mobile phase B: H₂O/ACN/HFIP/DIEA (35:65:0.75:0.0375, v:v:v:v) with 10 µM EDTA. The column used was a DNAPac RP column (4 µm, 50 × 2.1 mm, Thermo Fisher Scientific). Column temperature was set at 90 °C, and flow rate was 0.2–0.3 ml min⁻¹. The gradient started with 10% B, progressed to 50% B over 2.5 minutes and then increased to 100% B in 0.2 minutes and maintained for 0.8 minutes; the column was then re-equilibrated with 10% B for 1.5 minutes. A Dionex Ultimate 3000 HPLC system (Thermo Fisher Scientific) in combination with an Accela Open Autosampler (Thermo Fisher Scientific) and a Q Exactive mass spectrometer (Thermo Fisher Scientific) was used for the LC-HRMS analysis. The oligonucleotides were analyzed in negative ionization mode. The mass spectrometer was set at parallel reaction monitoring mode.

Histopathology, IHC and ISH. All animals were killed in accordance with AVMA Guidelines for the Euthanasia of Animals. Tissues were collected⁵² and fixed in

10% neutral-buffered formalin, processed routinely and stained with hematoxylin and eosin (H&E) as described previously¹⁰. H&E-based microscopic findings were recorded in the Pristima version 7.0.0 system (Xybion) and graded on a scale of 1–5 (1 = minimal, 2 = mild, 3 = moderate, 4 = marked, 5 = severe) by a board-certified veterinary pathologist.

Luxol fast blue/cresyl-echt violet (LFB/CEV) stain for myelin was performed on spinal cord, brainstem and cerebellum. In brief, de-paraffinized sections were dehydrated through three changes in xylene, 2 minutes each, and rehydrated through two changes of 100% and 95% ethanol, 2 minutes each. Sections were stained with 0.1% LFB (StatLab) either for 1 hour at 60 °C or overnight at room temperature, followed by 3–5 rinses in 95% ethanol, distilled water and differentiation in 0.05% lithium carbonate for 3–5 seconds. Next, sections were rinsed in distilled water, followed by counterstaining with CEV for 10 minutes, dehydrated through graded alcohols and xylene and routinely coverslipped. Decreases in LFB staining intensity and increases in IBA1 staining indicative of microgliosis were semi-quantitatively scored on a scale of 1–4 (1 = minimal, 2 = mild, 3 = moderate, 4 = marked).

IHC and ISH were performed on the Discovery Ultra automated instrument (Ventana Medical Systems) using manufacturer-provided reagents and protocols. For IHC, antibodies against the following targets were used: IBA1 1:1,600 (019-19741, Fujifilm Wako), GFAP 1:4,000 (Z0334, Agilent-Dako), CD31 1:75 (ab23874, Abcam), MAP2 1:1,000 (ab5392, Abcam), TTR 1:800 (prealbumin, SC-8104, Santa Cruz Biotechnology) and in-house anti-siRNA rabbit polyclonal antibody ab19151 at 1:12,000. The anti-siRNA antibody was isolated from rabbits dosed with Keyhole limpet hemocyanin (KLH)-conjugated fully modified siRNA mixed with Freund's adjuvant. *Iba1*, *Gfap* and *Pecam1* were detected with anti-rabbit NP multimer, followed by anti-NP AP multimer and Discovery Yellow or Discovery Purple AP Chromagen (all Ventana Medical Systems). MAP2 was detected with goat anti-chicken antibody (6100-08, Southern Biotech), followed by anti-goat HRP secondary antibody and Discovery Green HRP Chromogen (both Ventana Medical Systems). TTR was detected by anti-goat HRP secondary antibody, followed by Discovery Purple HRP Chromogen (both Ventana Medical Systems). siRNA was detected with anti-rabbit HRP secondary antibody, followed by Discovery Purple HRP Chromogen (Ventana Medical Systems). For ISH, sections were hybridized with a *Sod1* mRNA probe (Advanced Cell Diagnostics, 428589), followed by detection with RNAScope DAB amplification kit (Advanced Cell Diagnostics, 323200) and visualization with mRNA DAB Chromogen (Ventana Medical Systems).

Human whole blood cytokine release assay. Whole blood from four healthy human donors was collected into 10-ml sodium heparin Vacutainer tubes (Becton Dickinson), diluted 1:1 (v:v) in 0.9% saline (Baxter International) and added to 96-well tissue culture plates at a volume of 180 µl per well. siRNAs were transfected within 2 h of collection at a final concentration of 300 nM using 8 µg ml⁻¹ of DOTAP. After overnight incubation, plasma was collected for cytokine multiplex analysis (IL-1 β , IL-1RA, IL-6, IL-8, G-CSF, IP-10, MIP1 α and TNF- α) using Bio-Plex Pro assay kits (Bio-Rad).

Reporting summary. Further information on research design is available in the Nature Research Reporting Summary linked to this article.

Data availability

All datasets generated and analyzed in the study are provided within the manuscript files. Source data are provided with this paper.

References

- Beaucage, S. L. Solid-phase synthesis of siRNA oligonucleotides. *Curr. Opin. Drug Discov. Dev.* **11**, 203–216 (2008).
- Zhang, L., Peritz, A. & Meggers, E. A simple glycol nucleic acid. *J. Am. Chem. Soc.* **127**, 4174–4175 (2005).
- Zhang, L., Peritz, A. E., Carroll, P. J. & Meggers, E. Synthesis of glycol nucleic acids. *Synthesis* **2006**, 645–653 (2006).
- Schlegel, M. K. & Meggers, E. Improved phosphoramidite building blocks for the synthesis of the simplified nucleic acid GNA. *J. Org. Chem.* **74**, 4615–4618 (2009).
- O'Shea, J. et al. An efficient deprotection method for 5'-[O,O-bis(pivaloyloxymethyl)]-(E)-vinylphosphonate containing oligonucleotides. *Tetrahedron* **74**, 6182–6186 (2018).
- Kohonen, P. et al. A transcriptomics data-driven gene space accurately predicts liver cytopathology and drug-induced liver injury. *Nat. Commun.* **8**, 15932 (2017).
- Davis, J. et al. Early-onset and robust cerebral microvascular accumulation of amyloid β -protein in transgenic mice expressing low levels of a vasculotropic Dutch/Iowa mutant form of amyloid β -protein precursor. *J. Biol. Chem.* **279**, 20296–20306 (2004).
- Laubach, V. E., Foley, P. L., Shockey, K. S., Tribble, C. G. & Kron, I. L. Protective roles of nitric oxide and testosterone in endotoxemia: evidence from NOS-2-deficient mice. *Am. J. Physiol.* **275**, H2211–H2218 (1998).

50. Li, J. et al. Discovery of a novel deaminated metabolite of a single-stranded oligonucleotide in vivo by mass spectrometry. *Bioanalysis* **11**, 1955–1965 (2019).
51. Liu, J. et al. Oligonucleotide quantification and metabolite profiling by high-resolution and accurate mass spectrometry. *Bioanalysis* **11**, 1967–1980 (2019).
52. Bolon, B. et al. STP position paper: recommended practices for sampling and processing the nervous system (brain, spinal cord, nerve, and eye) during nonclinical general toxicity studies. *Toxicol. Pathol.* **41**, 1028–1048 (2013).

Acknowledgements

The authors thank Alnylam's Medicinal Chemistry Team, Medium Scale Synthesis Team, High Throughput Synthesis Team and Duplex Annealing Team for siRNA synthesis. They also thank A. Bisbe, P. Miller and R. Malone for siRNA purification; C. Wong, S. Maczko, M. Mendez, I. Duarte and D. Rooney for in vivo study support; A. Guan for tissue processing; J. Varao for sample management; B. Fitzsimmons for tissue drug concentration analysis; B. Carito, P. Gedman, C.-E. Stephany and K. Bittner for histology support; Alnylam's Research Analytical Team for metabolic stability studies; and the research team at CRL Finland, especially J. Puolivali and F. Khan.

Author contributions

K.M.B., J.K.N., M.M.J., S.M., M.K., C.B., D.F., K.F., M.A.M. and V.J. conceived the projects. K.M.B., J.K.N., M.M.J., S.M., Y.I.A.-R., L.T.H.D., H.P., C.S.T., E.C.-R., C.B., D.F.,

J.K., J.A., A.C., M.K.S., I.Z., M.K., M.A.M. and V.J. contributed to experimental design. L.T.H.D., H.P., C.S.T., E.C.-R., C.B., D.F., J.K., J.A., R.M., J.L., S.M., M.S., T.C., M.J., K.W., J.R., L.W., A.K., D.G., M.W.M., J.P., R.M., T.R., J.B., D.C., S.A., L.J., Y.J., S.L., J.G., T.N., S.C., S.L.B., U.P., A.K., A.B.R. and S.C. contributed experimentally. R.M., J.E.S. and W.D. provided non-human primate evaluations. C.S.T., T.C., K.W., J.R. and L.W. synthesized the duplexes. K.M.B., J.K.N., M.M.J., Y.I.A.-R., L.T.H.D., M.M., K.F., J.-T.W., M.A.M. and V.J. wrote the manuscript.

Competing interests

All authors are, or were during the time this work was conducted, employees of Alnylam Pharmaceuticals, with salary and stock options.

Additional information

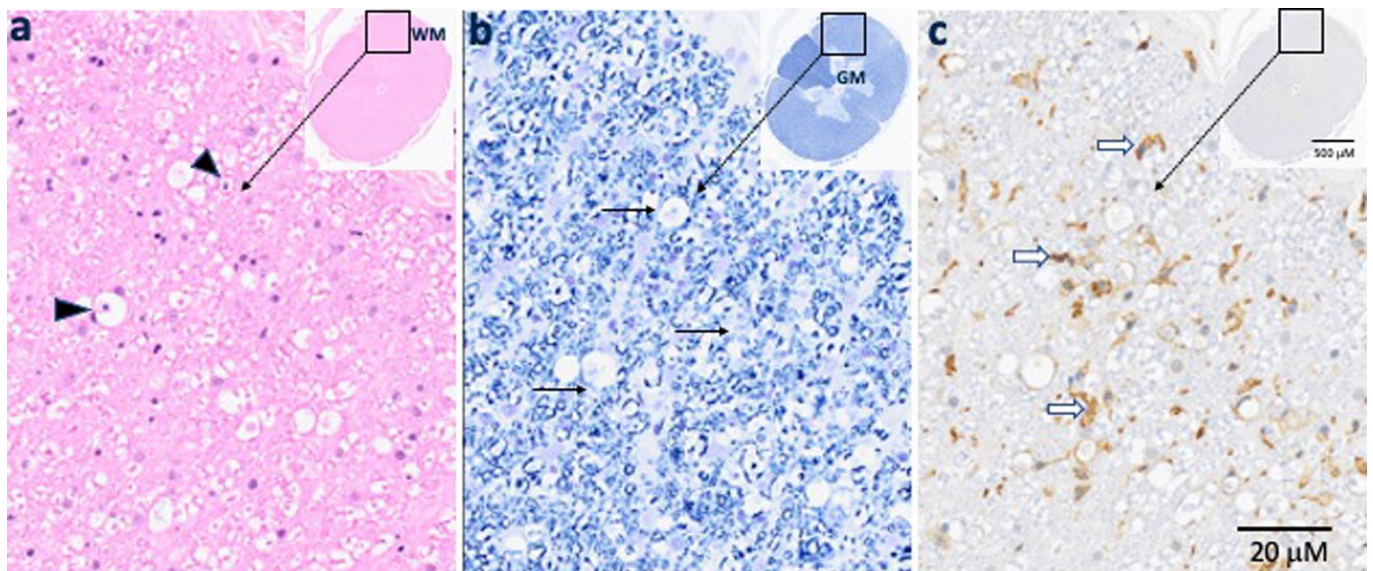
Extended data is available for this paper at <https://doi.org/10.1038/s41587-022-01334-x>.

Supplementary information The online version contains supplementary material available at <https://doi.org/10.1038/s41587-022-01334-x>.

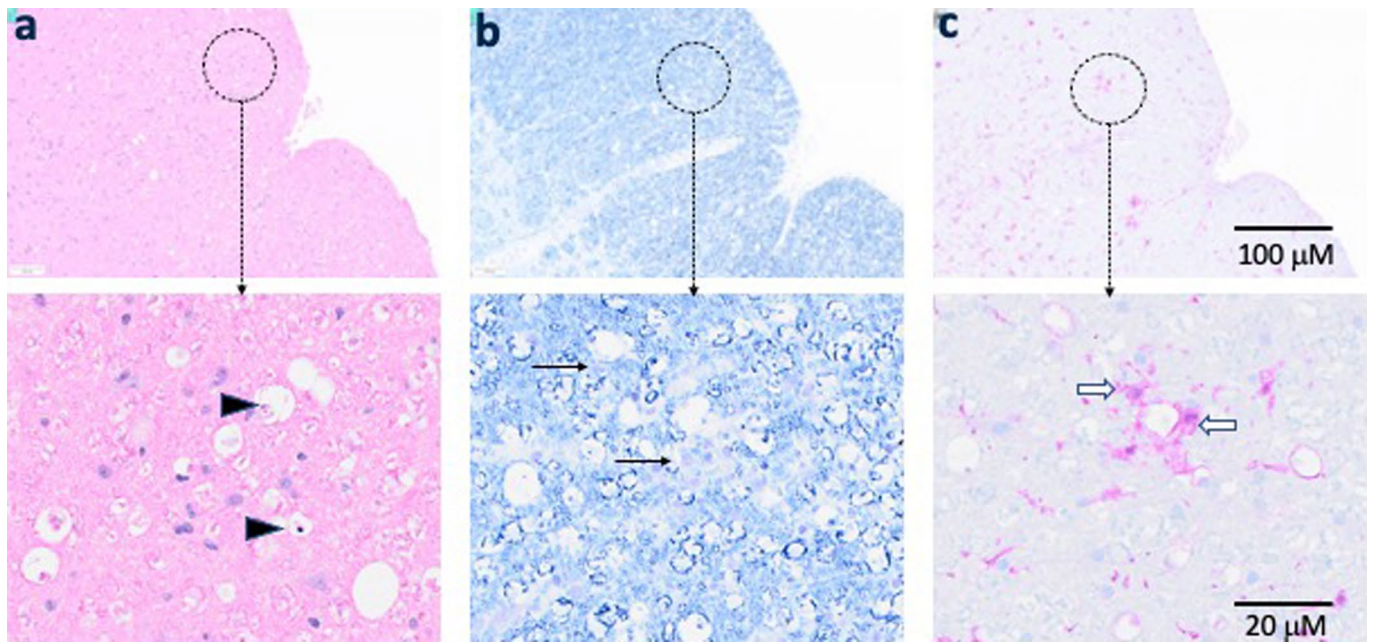
Correspondence and requests for materials should be addressed to Martin A. Maier or Vasant Jadhav.

Peer review information *Nature Biotechnology* thanks the anonymous reviewers for their contribution to the peer review of this work.

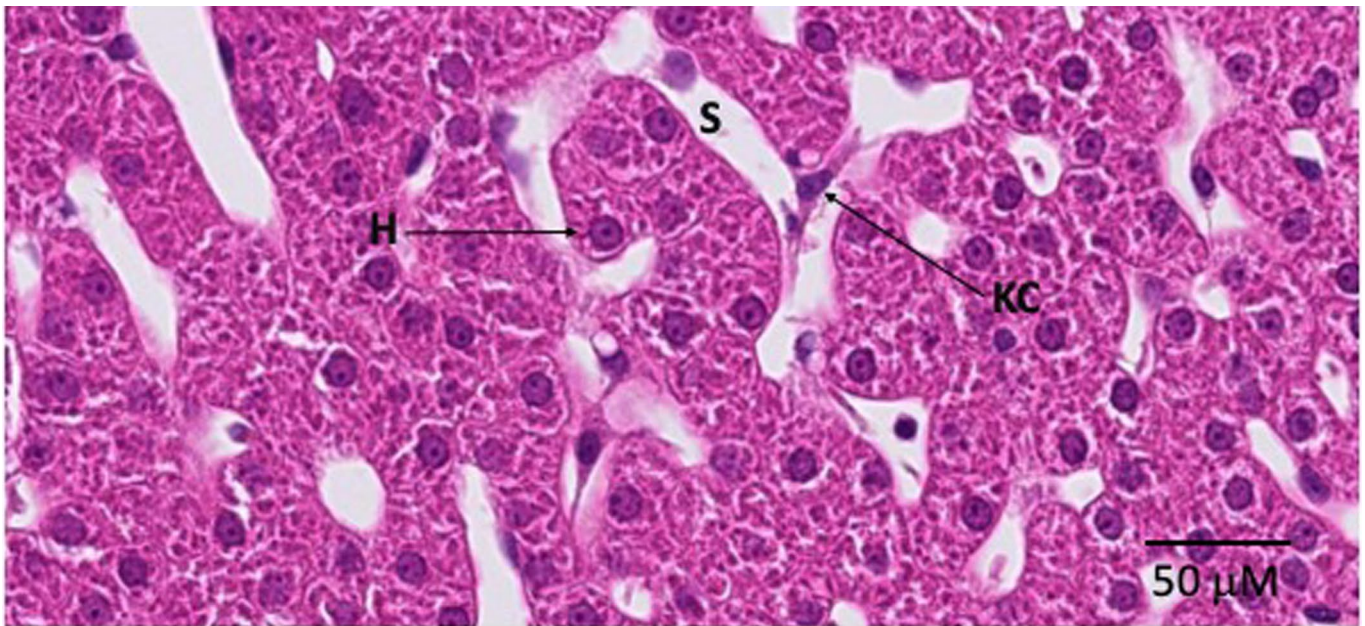
Reprints and permissions information is available at www.nature.com/reprints.



Extended Data Fig. 1 | Histopathological evaluation of the nonhuman primate (NHP) spinal cord at three months following a single IT dose of 60 mg C16-siRNA. Representative H&E (a), LFB (b) and IBA-1 (c) staining of NHP thoracic spinal cord. Microscopic findings in the spinal cord were limited to procedure-related changes (that is, IT bolus administration in lumbar region). These consisted of minimal to mild degeneration of nerve fibers with dilated axonal sheaths and few digestion chambers containing gitter cells (arrowheads) that were localized to the white matter of spinal cord (cervical, thoracic, and lumbar segments). Limited to procedure-affected areas, there were minimal decreases in LFB staining intensity (arrows) and a minimal increase in the number of IBA-1 (brown chromogen) positive microglia (open arrows). Three animals were analyzed per group with similar results. GM = grey matter; WM = white matter.



Extended Data Fig. 2 | Histopathological evaluation of the nonhuman primate (NHP) brain at three months following a single IT dose of 60 mg C16-siRNA. Representative H&E (a), LFB (b) and IBA-1 (c) staining of NHP brainstem (medulla oblongata region adjacent to aqueduct and underlying pons). Microscopic findings in the brain were limited to procedure-related changes (that is, CSF collection from cisterna magna). These consisted of minimal to mild degeneration of nerve fibers with dilated axonal sheaths and few digestion chambers containing gitter cells (arrowheads) that were localized to the peripheral white matter areas. Limited to procedure-affected areas, there were minimal decreases in LFB staining intensity (arrows) and a minimal increase in the number of IBA-1 (purple chromogen) positive microglia (open arrows). Three animals were analyzed per group with similar results.



Extended Data Fig. 3 | Histopathological evaluation of the nonhuman primate (NHP) liver at three months following a single IT dose of 60 mg C16-siRNA. Representative H&E staining of NHP liver (H = hepatocyte; S = sinusoid; KC = Kupffer cell). There were no remarkable microscopic findings. Three animals were analyzed per group with similar results.

Reporting Summary

Nature Research wishes to improve the reproducibility of the work that we publish. This form provides structure for consistency and transparency in reporting. For further information on Nature Research policies, see our [Editorial Policies](#) and the [Editorial Policy Checklist](#).

Statistics

For all statistical analyses, confirm that the following items are present in the figure legend, table legend, main text, or Methods section.

n/a Confirmed

- The exact sample size (n) for each experimental group/condition, given as a discrete number and unit of measurement
- A statement on whether measurements were taken from distinct samples or whether the same sample was measured repeatedly
- The statistical test(s) used AND whether they are one- or two-sided
Only common tests should be described solely by name; describe more complex techniques in the Methods section.
- A description of all covariates tested
- A description of any assumptions or corrections, such as tests of normality and adjustment for multiple comparisons
- A full description of the statistical parameters including central tendency (e.g. means) or other basic estimates (e.g. regression coefficient) AND variation (e.g. standard deviation) or associated estimates of uncertainty (e.g. confidence intervals)
- For null hypothesis testing, the test statistic (e.g. F , t , r) with confidence intervals, effect sizes, degrees of freedom and P value noted
Give P values as exact values whenever suitable.
- For Bayesian analysis, information on the choice of priors and Markov chain Monte Carlo settings
- For hierarchical and complex designs, identification of the appropriate level for tests and full reporting of outcomes
- Estimates of effect sizes (e.g. Cohen's d , Pearson's r), indicating how they were calculated

Our web collection on [statistics for biologists](#) contains articles on many of the points above.

Software and code

Policy information about [availability of computer code](#)

Data collection *No software was used for data collection*

Data analysis *Graphpad prism version 8.2.1*

For manuscripts utilizing custom algorithms or software that are central to the research but not yet described in published literature, software must be made available to editors and reviewers. We strongly encourage code deposition in a community repository (e.g. GitHub). See the Nature Research [guidelines for submitting code & software](#) for further information.

Data

Policy information about [availability of data](#)

All manuscripts must include a [data availability statement](#). This statement should provide the following information, where applicable:

- Accession codes, unique identifiers, or web links for publicly available datasets
- A list of figures that have associated raw data
- A description of any restrictions on data availability

The datasets generated during and/or analysed during the current study are available from the corresponding author on reasonable request.

Field-specific reporting

Please select the one below that is the best fit for your research. If you are not sure, read the appropriate sections before making your selection.

Life sciences Behavioural & social sciences Ecological, evolutionary & environmental sciences

For a reference copy of the document with all sections, see [nature.com/documents/nr-reporting-summary-flat.pdf](https://www.nature.com/documents/nr-reporting-summary-flat.pdf)

Life sciences study design

All studies must disclose on these points even when the disclosure is negative.

Sample size	The described animal studies generally utilized 3-4 animals per group per 3Rs principles.
Data exclusions	No data were excluded.
Replication	The described animal studies were not replicated per 3Rs principles. The average and mean for each group of animals is presented.
Randomization	The animals were randomized based on body weight.
Blinding	The rodent studies were dosed by one group, and the tissues were transferred to another group for analysis. The NHP studies were dosed at CROs, and the tissues were transferred to Alnylam for analysis.

Reporting for specific materials, systems and methods

We require information from authors about some types of materials, experimental systems and methods used in many studies. Here, indicate whether each material, system or method listed is relevant to your study. If you are not sure if a list item applies to your research, read the appropriate section before selecting a response.

Materials & experimental systems

Methods

n/a	Involved in the study	n/a	Involved in the study
<input type="checkbox"/>	<input checked="" type="checkbox"/> Antibodies	<input checked="" type="checkbox"/>	<input type="checkbox"/> ChIP-seq
<input type="checkbox"/>	<input checked="" type="checkbox"/> Eukaryotic cell lines	<input checked="" type="checkbox"/>	<input type="checkbox"/> Flow cytometry
<input checked="" type="checkbox"/>	<input type="checkbox"/> Palaeontology and archaeology	<input checked="" type="checkbox"/>	<input type="checkbox"/> MRI-based neuroimaging
<input type="checkbox"/>	<input checked="" type="checkbox"/> Animals and other organisms		
<input checked="" type="checkbox"/>	<input type="checkbox"/> Human research participants		
<input checked="" type="checkbox"/>	<input type="checkbox"/> Clinical data		
<input checked="" type="checkbox"/>	<input type="checkbox"/> Dual use research of concern		

Antibodies

Antibodies used	The following antibodies were used for IHC and are described in the methods: IBA1 1:1600 (#019-19741, Fujifilm Wako, Richmond, VA), GFAP 1:4000 (#Z0334, Agilent-Dako, Santa Clara, CA), CD31 1:75 (#ab23874, Abcam, Waltham, MA), MAP2 1:1000 (#ab5392, Abcam), TTR 1:800 (prealbumin, #SC-8104, Santa Cruz Biotechnology, Dallas, TX), and in-house anti-siRNA rabbit polyclonal antibody ab19151 at 1:12000. The following antibodies were used for ELISA and are described in the methods: sAPP α and sAPP β (Meso Scale Discovery, K15120E), rabbit anti-human TTR pAb (Dako, A0002), and anti-hTTR pAb (Abcam, ab9015).
Validation	The antibodies were validated utilizing tissues known to lack or express the analyte of interest. Morphological confirmation of expression in a specific cell type within a tissue was used as an additional validation.

Eukaryotic cell lines

Policy information about [cell lines](#)

Cell line source(s)	Rat RPE-J cells (ATCC, CRL-2240)
Authentication	No authentication
Mycoplasma contamination	Not tested for mycoplasma contamination
Commonly misidentified lines (See ICLAC register)	None

Animals and other organisms

Policy information about [studies involving animals](#); [ARRIVE guidelines](#) recommended for reporting animal research

Laboratory animals	Mouse (C57BL/6, female, 8-10 weeks), Rat (Sprague Dawley, male, 8-10 weeks), Monkey (Cynomolgus, male and female, 1.5-3 years), homozygous Tg-hAPP ^{SwDI} /mNos2 ^{-/-} (referred to as CVN mice, male and female 6-12 months)
Wild animals	None
Field-collected samples	None
Ethics oversight	All studies were conducted using protocols consistent with local, state and federal regulations, as applicable, and approved by the Institutional Animal Care and Use Committee (IACUC) at Alnylam Pharmaceuticals, Charles River Laboratories (CRL), or LabCorp (formerly Covance, Inc.), as applicable.

Note that full information on the approval of the study protocol must also be provided in the manuscript.